jmr&t
Journal of Materials Research and Technology
www.jmrt.com.br

Original article

Microstructure of nitrided and nitrocarburized layers produced on a superaustenitic stainless steel

Frederico Augusto Pires Fernandes[a], *Luiz Carlos Casteletti*[a], *Juno Gallego*[b,*]

[a] *Department of Materials Engineering, Escola de Engenharia de São Carlos, Universidade de São Paulo (EESC/USP), São Carlos, SP, Brazil*
[b] *Department of Mechanical Engineering, Universidade Estadual Paulista (UNESP), Ilha Solteira, SP, Brazil*

ARTICLE INFO

Article history:
Received 5 December 2012
Accepted 31 January 2013
Available online 14 June 2013

Keywords:
Nitriding
Nitrocarburizing
Superaustenitic stainless steel
Expanded austenite
Microstructure
Transmission electron microscopy

ABSTRACT

The expanded austenite γ_N can be produced in austenitic stainless steels by plasma nitriding, carburizing or nitrocarburizing at low temperatures. This metastable phase presents higher hardness and toughness if compared with traditional nitride layers whilst also maintaining the corrosion resistance. However, the application of plasmas composed by both nitrogen and carbon is technologically recent and the effect of such process on the microstructure and properties of the nitrocarburized layers is still under investigation. In this study, samples of UNS S31254 superaustenitic stainless steel were produced by plasma nitriding and nitrocarburizing at 400 °C, 450 °C and 500 °C for 5 h. The plasma treated samples were observed by optical and transmission electron microscopy and also analyzed by X-ray diffraction. The thickness of the layers increased with temperature and the nitrocarburized layers were thicker than nitrided at a given temperature. The presence of expanded austenite was confirmed by X-ray diffraction through its characteristic anomalous shift on the diffracted peaks related to the austenite. Nitride formation on samples produced at 400 °C was only identified by transmission electron microscopy where fine rounded particles with 10–15 nm size revealed reflections consistent with the CrN cubic chromium nitride. The estimated lattice parameter from the expanded austenite ranged from 0.38 to 0.41 nm depending on the employed $\{hkl\}$ reflection which was found to be 6–11% larger than the untreated austenite lattice parameter.

1. Introduction

Superaustenitic stainless steels (SASSs) are materials extensively applied on components demanding high corrosion resistance in which its wear and fatigue resistance can be improved by a thermochemical surface engineering method such as plasma nitriding (PN) or plasma nitrocarburizing (PNC) [1]. When performed at relatively low temperatures, below 500 °C, the result is a surface layer with high hardness and wear resistance that does not compromise the corrosion properties of the austenic stainless steel substrate [2,3]. Such layer is frequently referred as S-phase or expanded austenite γ_N and is originated by interstitial (N and/or C) super-saturation of the austenitic matrix where it remains in solid solution at octahedral sites from the crystalline face-centered cubic lattice. The

* *Corresponding author.*
E-mail addresses: gallego@dem.feis.unesp.br, jgallego.dem@gmail.com (J. Gallego).
2238-7854 http://dx.doi.org/10.1016/j.jmrt.2013.01.007

Table 1 – Chemical composition (wt.%) of the UNS S31254 SASS.

C	Mn	Si	Cr	Ni	Mo	N	Cu	Fe
0.020	0.90	0.50	20.23	18.25	6.08	0.20	0.69	Bal.

presence of the interstitial elements above the solubility limit (from 30 to 40 at.%) results in a highly distorted structure and thermodynamically meta-stable [4–8].

The distortion of the lattice caused by an enormous amount of interstitial elements on the expanded austenite layer generates compressive residual stresses that enhance diffusion and also contributes to the production of stacking faults. Another consequence from the nitrogen and/or carbon super-saturation relates to the crystallography of the S-phase which shows an anomalous behavior when probed by X-ray diffraction (XRD) [9–12]. XRD spectra attained for this phase present a low-angle anisotropic shift of the Bragg reflections when compared to expected ones obtained for a hypothetically uniformly expanded austenite. Thus {1 0 0} peaks indicate larger lattice parameters than those calculated for the {1 1 1}. The elastic distortion of the austenite lattice plus the impressive amount of stacking faults promote broadening on the diffracted peaks which makes the identification of phases with low volumetric fraction (such as chromium and iron nitrides) more complex. Analyzing thin foils by transmission electron microscopy (TEM) allows the identification of phases with small size and quantity. Besides that it enables a crystallographic analysis of nanometric regions of a sample. In the present work PN and PNC treatments were performed on specimens from a superaustenitic stainless steel under different temperatures. XRD analyses confirmed the presence of the expanded austenite on the produced layers although only the TEM technique was able to identify the fine precipitation of chromium nitrides. The appearance of such particles is attributed to a local decomposition of the expanded austenite during the thermochemical treatments.

2. Experimental procedure

Pieces of 20 mm diameter and 3 mm thickness were machined from a commercial round bar of UNS S31254 SASS whose chemical composition is given in Table 1. Polished surfaces for PN and PNC were prepared after wet grinding with sandpaper up to 1500 grit and final mechanical polishing with 1.0 μm alumina. Surface sputtering in a 500 Pa pure argon atmosphere was performed during 0.5 h at 50 °C lower than plasma treatment carried out at 400 °C, 450 °C or 500 °C for 5 h. The PN and PNC atmospheres were composed respectively of 80% H_2–20% N_2 and 77% H_2–20% N_2–3% CH_4 by volume [13].

Small pieces were carefully cut from the nitrided and nitrocarburized layers for preparation of conventional cross-sectional metallographic samples, which were observed under Zeiss® Axiotech optical microscope after etching in a fresh solution containing 75 mL hydrochloric acid and 25 mL nitric acid (aqua regia etchant). Vickers microhardness measurements were carried out using Buehler® digital equipment with 490 mN (50 gf) load during 10 s. At least six measurements were considered for each sample statistics, where dispersion is represented by standard deviation.

Identification of microconstituents in the substrate, PN and PNC layers were determined with a Rigaku® Geigerflex diffractometer (Bragg–Brentano configuration) using Cu-Kα radiation

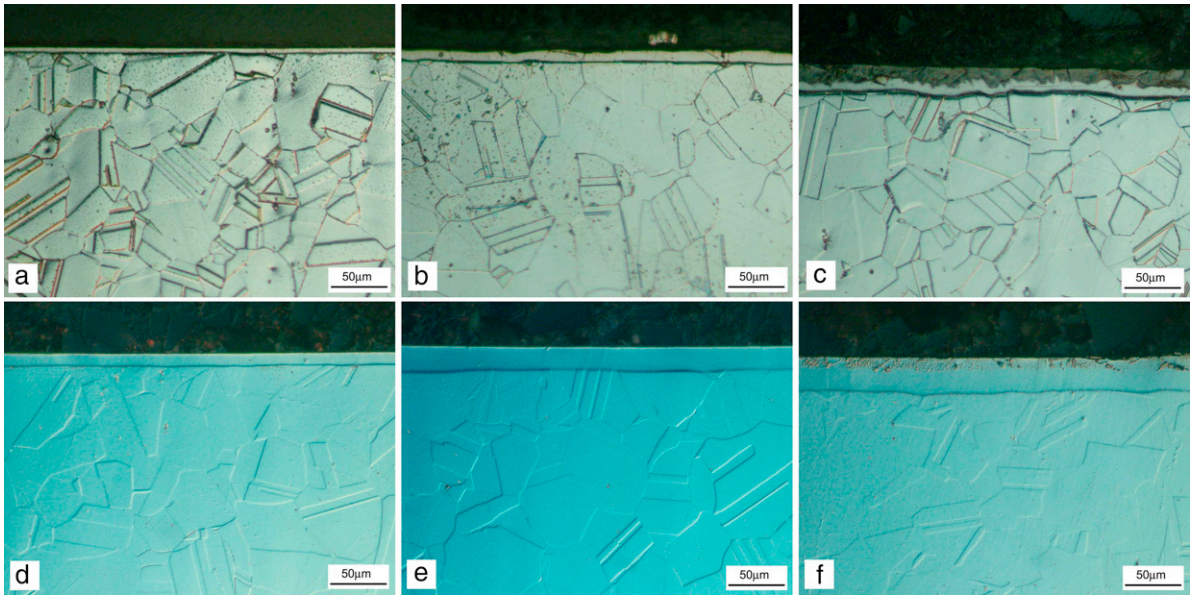

Fig. 1 – Optical micrographs showing cross section of PN (a–c) and PNC (d–f) layers formed after 5 h at 400 °C (a and d), 450 °C (b and e) and 500 °C (c and f). Etching: aqua regia.

(λ = 154.05 pm) and graphite monochromator. The diffracted intensity was recorded between 30° and 100° 2θ range, swept with speed of 2°/min. Diffracted reflections obtained from XRD patterns were compared with crystallographic information files available from the inorganic crystal structure database (ICSD) [14].

TEM was applied to investigate a plan-view section of PN and PNC layers, where the treated surface of the thin foil sample was normal to the incident electron beam. The substrate side of treated samples was carefully ground up to 150 μm thick when 3.0 mm diameter disks were punched with an appropriate mechanical device. A transparent thick lacquer protective layer was deposited on the treated surface to prevent its degradation during TEM sample preparation. Thin foils were obtained by one-side jet electro-polishing where a 5% perchloric acid–95% acetic acid solution (by volume) at room temperature was used under a polishing potential/current of 40 V/40 mA, respectively. The TEM observations were performed in a Philips® CM120 microscope operated at 120 kV (λ = 3.35 pm) and equipped with an EDS microanalysis device. EDS counting was performed during 100 s live time where the spot size of the electron beam was adjusted to give a detecting dead time between 20% and 40%. Crystallographic parameters were determined from selected area electron diffraction patterns (SAED), using a standard calibrated camera length [15].

3. Results and discussion

In Fig. 1 the typical cross sections from the plasma nitrided (Fig. 1a–c) and nitrocarburized (Fig. 1d–f) layers of the SASS treated at 400 °C, 450 °C and 500 °C for 5 h are shown. Below all produced layers the austenitic matrix is seen and composed by grains with polygonal morphology and size between 50 and 100 μm in which annealing twins are noticed. Over the surface of the specimens uniform layers are identified indicating that thickness of the layers increased with temperature like depicted in Fig. 2a. It is also readily observed that for a given temperature PNC produced thicker layers than nitriding. Such observation is attributed to the fact that carbon diffuses faster than nitrogen on austenite. Besides that nitrogen becomes readily trapped in octahedral sites from the FCC lattice due to its high chemical affinity with chromium in solid solution [7]. Both nitriding and nitrocarburizing treatments performed at 500 °C show the occurrence of a complex thicker layer composed of more than one phase that is easily noticed by the dark etched regions on the cross sections (Fig. 1c and f). According to the literature [9] this dark layer is mainly composed by chromium nitrides which impair the corrosion resistance. The contrast derived from the optical microscopy also suggests that nitrides have precipitated on the sample nitrided at 450 °C (Fig. 1b). The nucleation of these secondary nitride phases starts much probably on the surface where nitrogen concentration is higher and then growing inwards through the layer.

Vickers hardness measurements presented in Fig. 2b show that the layers produced by nitriding and nitrocarburizing at higher temperatures result in a considerable increase on the surface hardness level. This occurs due to the super-saturation

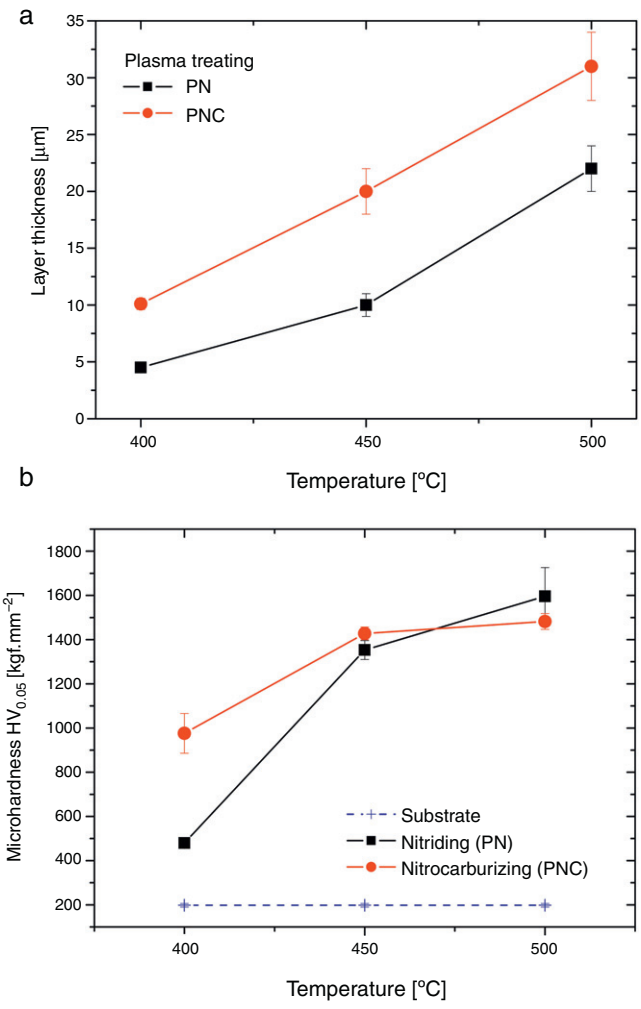

Fig. 2 – Effect of treating temperature on thickness (a) and Vickers microhardness (b) of PN and PNC layers produced on SASS.

of the surfaces with interstitial elements such as carbon and/or nitrogen after the plasma treatment. The scattering on the hardness measurements might be associated to the heterogeneity of the layers since the dispersion of the phases expanded austenite/nitrides were not well uniform for the temperatures of 450 °C and 500 °C. The increase on the layer fragility with temperature also promotes formation of cracks and micro-cavities what could have caused variations on the measured values. The differences on the measurements from the layers produced above 450 °C were not statistically significant.

XRD patterns obtained from SASS substrate and PN/PNC layers are presented in Fig. 3. The reflections indicated by the substrate are very consistent with FCC austenite reported in ICSD 53803 CIF card, where lattice parameter did not exceed 1% of the standard value. The diffracted intensity variation can be explained due to random occupation of the lattice points by different substitutional alloying elements and the effect of texture, introduced by the plastic deformation of the SASS rolled bars.

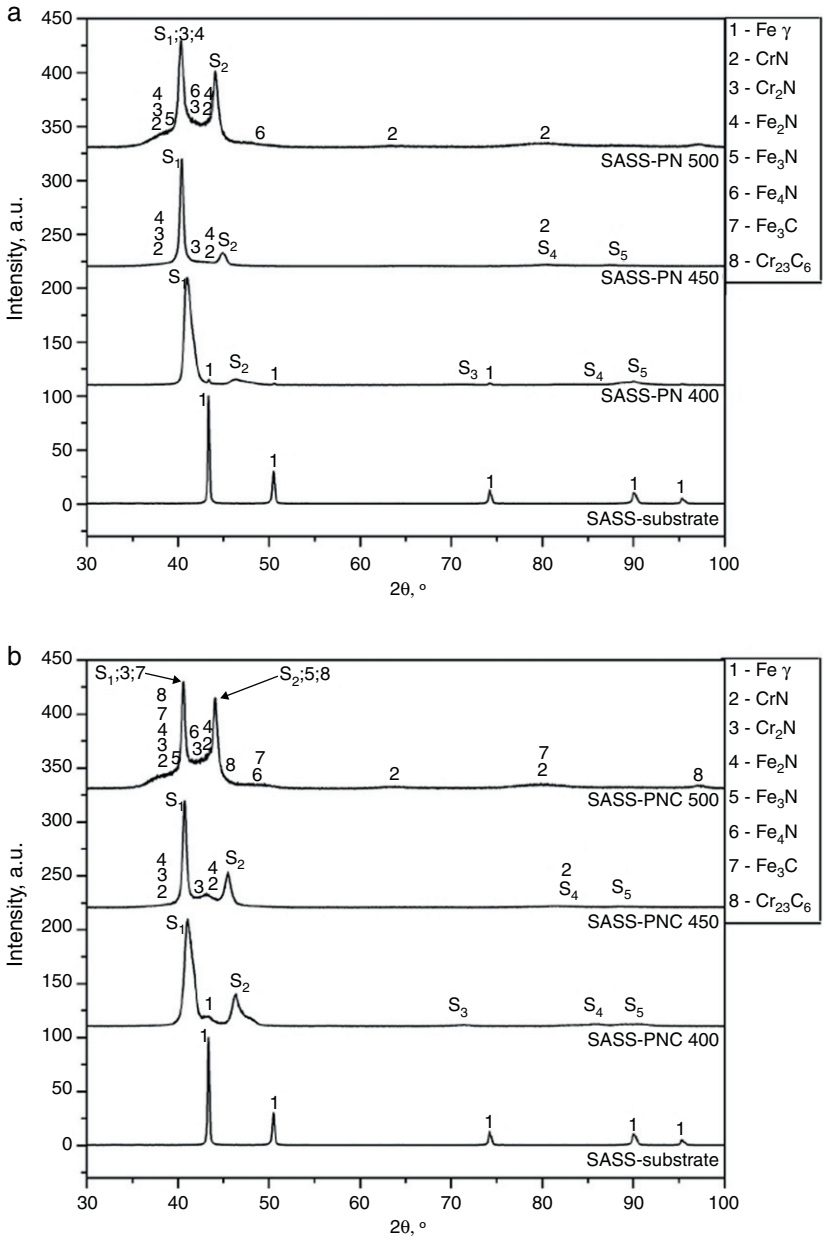

Fig. 3 – XRD patterns of PN (a) and PNC (b) layers formed at 400–500 °C on SASS samples. Cu-Kα radiation.

The expanded austenite γ_N is a thermodynamically metastable phase frequently observed in nitrided or nitrocarburized layers formed at low temperatures. The diffracted peaks of Fig. 3 related to this phase were marked by the letter 'S' and their identification was based on γ_N diffraction data reported elsewhere [16]. On samples nitrided at 400 °C the formation of expanded austenite is observed with additional weak diffraction peaks from the substrate. No significant XRD intensity from other phases was detected especially nitrides, whose presence may have been hidden by the peak broadening of expanded austenite and/or by its very small volume fraction. Increasing the nitriding temperature to 450 °C the presence of nitrides is not so evident what only occurs clearly in the sample treated at 500 °C. In fact the XRD results have confirmed the formation of a thin complex compound layer showed in micrographs Fig. 1c and f, composed by iron and chromium nitrides, in PN and PNC treatments performed at 500 °C. Similar XRD results were achieved for nitrocarburized samples.

In general $\{h\,k\,l\}$ reflections of the expanded austenite were positioned at lower 2θ Bragg angles, if compared to the same $\{h\,k\,l\}$ diffracted peak from the untreated austenite. That displacement in 2θ is not uniform and depends on the operative $\{h\,k\,l\}$ reflection. While $\{1\,1\,1\}$ austenite peak is positioned at 43.44° in Fig. 3a, corresponding γ_N reflection (S1 peak) displaces to 2θ angles of 41.64°, 40.44° and 40.32° in the samples nitrided at 400 °C, 450 °C and 500 °C, respectively. For nitrocarburized specimens, Fig. 3b, displacement of $\{1\,1\,1\}$ peaks was determined for 2θ angles corresponding to 40.76°, 40.68° and 40.60° for the samples treated, respectively, at 400 °C, 450 °C

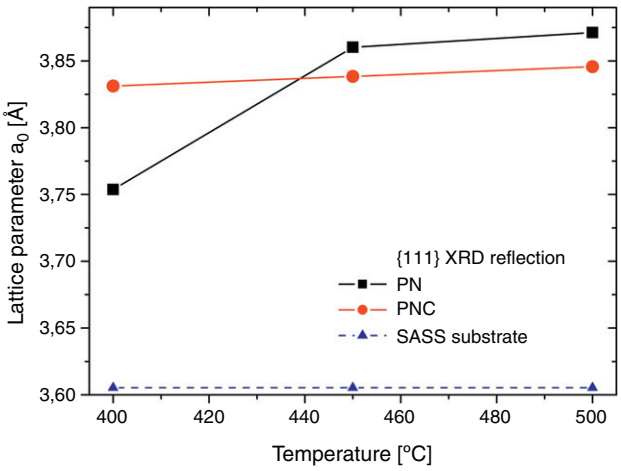

Fig. 4 – Effect of temperature on the lattice parameter estimated from {1 1 1} XRD reflection after PN and PNC treatments.

and 500 °C. According to Bragg's law these results indicate that lattice parameter is increasing gradually with the treatment temperature, as shown in Fig. 4.

As previously mentioned, the presence of the expanded austenite in a XRD pattern is usually characterized by broad diffracted peaks located at lower Bragg's angle than its corresponding reflection observed for the untreated austenite. Such behavior is the effect of the introduction of colossal amounts of nitrogen in austenite, which can reach 40 at.% and that is well above the solubility limit of the FCC matrix (10.3 at.%) [17]. The occupation of the octahedral sites in the FCC lattice increases with nitrogen concentration. The anisotropic diffusivity of interstitial solute [5] and decreasing of stacking faults energy promoted by the presence of nitrogen [12] are able to create elastic distortions on the crystalline lattice, whose effect yields the broadening of the diffracted peaks. The dispersion of chromium atoms in austenite, coupled with its strong chemical affinity with nitrogen and carbon, contributes to the permanence of the interstitial in the iron matrix. At lower plasma treatment temperatures, despite the colossal super-saturation of nitrogen, high chromium availability and lower enthalpy of formation [18], we should not expect intense nucleation of chromium nitrides. Due to thermodynamic and kinetic reasons [7] such nitrides are massively formed after longer treatments under higher temperatures, as confirmed by the XRD patterns presented in Fig. 3.

The observation of thin foils by TEM has showed the presence of dislocations and stacking faults in both nitrided and nitrocarburized layers produced on SASS treated at 400 °C. Such crystalline defects improve nitrogen and carbon mobility, favoring its introduction and diffusion in austenite [11]. The nitrided layers have usually shown a uniform microstructure, as depicted in Fig. 5a. The ring-type SAED pattern obtained suggests the presence of a large number of fine particles where the selected area diffraction aperture was positioned. In fact, Fig. 5b shows a dark field contrast of a large number of fine rounded particles (10–15 nm) found in the nitrided SASS layer whose diffracted reflection are consistent with {2 0 0} of cubic chromium nitride (CrN). These particles were not identified

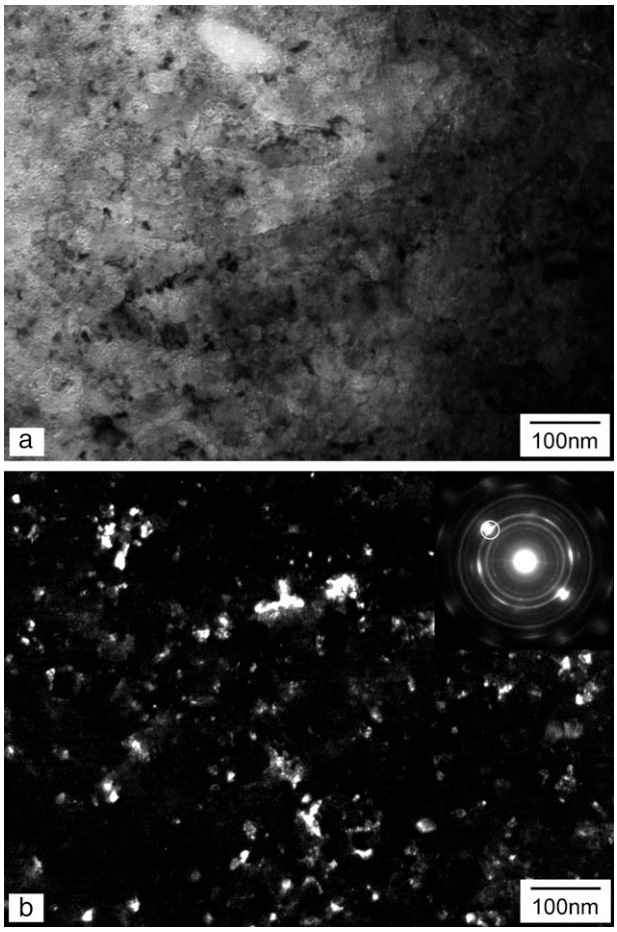

Fig. 5 – Thin foil TEM micrographs showing typical bright field (BF) contrast of nitrided layers formed at 400 °C in (a) and fine chromium nitride precipitation revealed by {2 0 0} reflection in same specimen (b).

by XRD due to its very small volume fraction. Similar results were obtained by TEM observation of thin foil samples prepared from nitrocarburized layer, Fig. 6a, where chromium and iron nitrides have presented some preferential orientation with expanded austenite matrix, as SAED pattern suggests in Fig. 6b.

Calculations involving several γ_N SAED patterns allowed to evaluate the expansion of the lattice parameter between 7% and 11% compared with untreated austenite. The dispersion of the results may be associated with an enlargement of the diffracted beams caused by nitrogen supersaturated solid solution in expanded austenite, which form quite diffuse spots in the SAED patterns [14]. Furthermore it can be considered that there are some differences in nitrogen and/or carbon concentration in each austenite grain, as a result of anisotropic diffusion of interstitial elements [5]. In addition to the formation of diffuse diffracted beams in SAED, massive amounts of interstitial promote twinning of austenitic matrix due to large elastic strains generated. Bundles of stacking faults and twins were observed by TEM in SASS nitrided layers (like described previously [16]) should have also contributed to the peak broadening in XRD patterns. The lattice parameters calculated by SAED were larger than those deter-

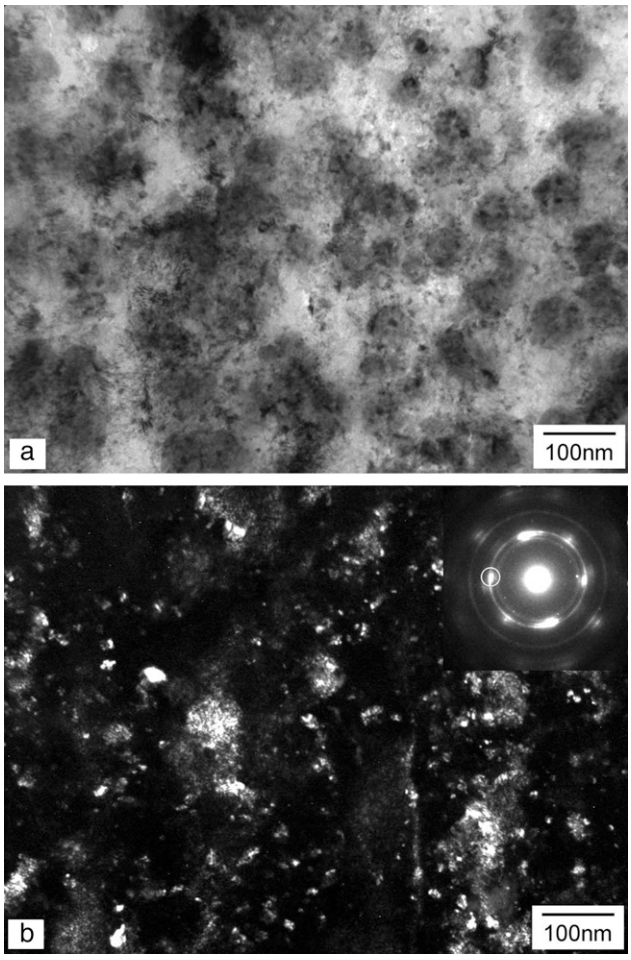

Fig. 6 – Thin foil TEM micrographs showing typical BF contrast of nitrocarburized layer formed at 400 °C in (a). Iron/chromium nitrides slightly texturized on expanded austenite layer are revealed by dark field contrast in (b).

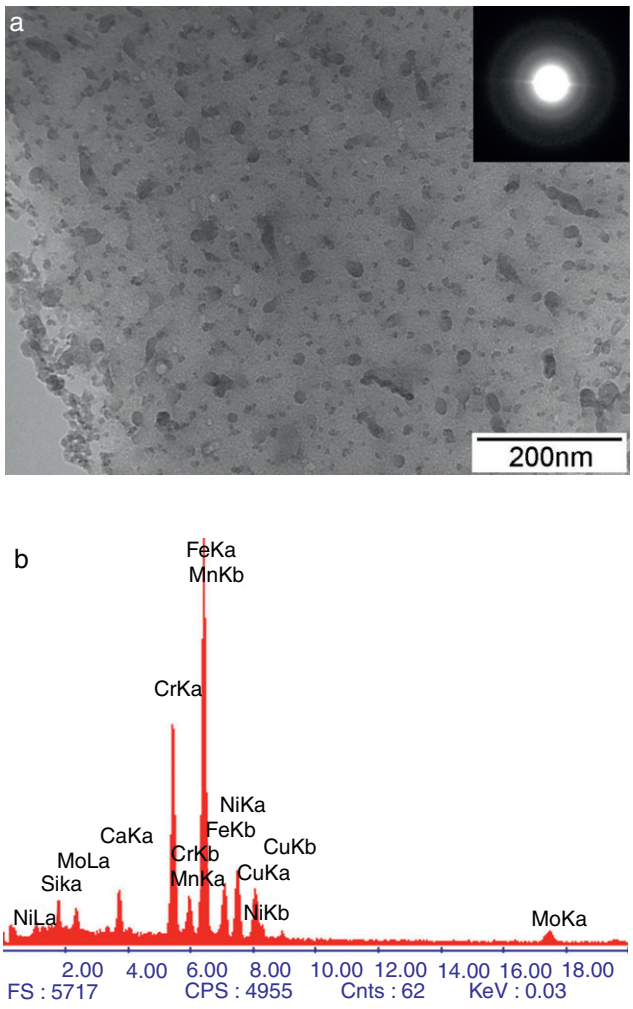

Fig. 7 – BF thin foil TEM micrograph showing amorphization of PNC layer formed at 400 °C in (a). Its metallic nature has been confirmed by EDS microanalysis (b).

mined by XRD. Those results were associated to the effect of substrate on the compressive residual stress resulting from thermochemical treatment. In the samples analyzed by electron diffraction there was a stress relief with removal of the substrate during electropolishing, in order to obtain suitable thin foils for TEM [19,20].

Lack of crystallinity (amorphization) of expanded austenite was occasionally observed in some regions of both PN and PNC layers as illustrated in the TEM bright field micrograph of Fig. 7a. Amorphous structures have typically exhibited a monotonous contrast, being crystallographically confirmed by presence of enlarged and diffused halos in their respective SAED patterns. The metallic nature of the amorphous regions was confirmed by EDS microanalysis, Fig. 7b, where the presence of significant amounts of typical alloying elements of SASS such as chromium, nickel and molybdenum have been observed. This rare and localized loss of crystallinity can be attributed to the effect of the massive introduction of nitrogen/carbon into the austenite matrix, associated with the low diffusivity of substitutional alloying elements, such as chromium and molybdenum, at lower PN/PNC treatment temperatures [21,22].

4. Conclusions

In this work the so-called 'expanded austenite' was obtained after PN and PNC of a UNS S31254 superaustenitic stainless steel at temperatures between 400 °C and 500 °C for 5 h. PNC has produced thicker layers than nitriding. The XRD analyses have shown that expanded austenite has an anomalous expanded crystalline structure in which the estimated lattice parameter for the {111} reflection was significantly smaller than that obtained for the {200}. The expansion levels on the crystalline lattice increased with treatment temperature and were slightly smaller for the nitrocarburized layers at higher temperatures (450 °C and 500 °C). The calculated expansion levels for the expanded austenite reached 7.4% and 6.7% for nitrided and nitrocarburized layers, respectively. Amorphization was rarely observed for nitrided and nitrocarburized samples studied by TEM. Much probably the introduction of colossal amounts of interstitial elements is responsible for the production crystalline defects and very fine chromium nitride

precipitation that were only identified by TEM and also contributed to the hardness increasing of the layers.

Conflicts of interest

The authors declare no conflicts of interest.

Acknowledgments

The authors thank the LCE/DEMa/UFSCar for TEM facilities and the grants awarded by CAPES (FAPF) and CNPq (LCC and JG) during the development of this work.

REFERENCES

[1] Bell T, Mao K, Sun Y. Surface engineering design: modelling surface engineering systems for improved tribological performance. Surf Coat Technol 1998;108/109:360–8.
[2] Zhu X, Huang H, Xu K, He J. Structure and properties of plasma nitrided austenitic stainless steel. In: Proceedings of the 20th ASM heat treating society conference. 2000. p. 217–21.
[3] Li XY. Low temperature plasma nitriding of 316 stainless steel: nature of "S" phase and its thermal stability. Surf Eng 2001;17:147–52.
[4] Menthe E, Rie K-T, Schultze JW, Simson S. Structure and properties of plasma nitrided stainless steel. Surf Coat Technol 2000;74/75:412–6.
[5] Rivière JP, Templier C, Declémy A, Redjdal O, Chumlyakov Y, Abrasonis G. Microstructure of expanded austenite in ion-nitrided AISI 316L single crystals. Surf Coat Technol 2007;201:8210–4.
[6] Christiansen T, Somers MAJ. On the crystallographic structure of S-phase. Scr Mater 2004;50:35–7.
[7] Williamson DL, Ozturk O, Wei R, Wilbur PJ. Metastable phase formation and enhanced diffusion in FCC alloys under high dose, high flux nitrogen implantation at high and low ion energies. Surf Coat Technol 1994;65:15–23.
[8] Sozinov AL, Balanyuk AG, Gavriljuk VG. N–N interaction and nitrogen activity in the iron base austenite. Acta Mater 1999;47:927–35.
[9] Dong H. S-phase surface engineering of Fe–Cr, Co–Cr and Ni–Cr alloys. Int Mater Rev 2010;55:65–98.
[10] Buhagiar J, Li X, Dong H. Formation and microstructural characterization of S-phase layers in Ni-free austenitic stainless steels by low-temperature plasma surface alloying. Surf Coat Technol 2009;204:330–5.
[11] Manova D, Eichentopf I-M, Hirsch D, Mändl S, Neumann H, Rauschenbach B. Influence of microstructure on nitriding properties of stainless steel. IEEE Trans Plasma Sci 2006;34:1136–40.
[12] Xu XL, Wang L, Yu ZW, Hei ZK. Microstructural characterization of plasma nitrided austenitic stainless steel. Surf Coat Technol 2000;132:270–4.
[13] Fernandes FAP, Heck SC, Pereira RG, Picon CA, Nascente PAP, Casteletti LC. Ion nitriding of a superaustenitic stainless steel: wear and corrosion characterization. Surf Coat Technol 2010;204:3087–90.
[14] Inorganic Crystal Structure Database. Crystallographic information files. Karlsruhe: ICSD; 2012. Available from: http://www.fiz-karlsruhe.de/icsd.html [cited 2012 May 12].
[15] Williams DB, Barry Carter C. Transmission electron microscopy: a textbook for materials science. 2nd ed. New York: Springer Science and Business Media LLC; 2009.
[16] Totten GE, Casteletti LC, Fernandes FAP, Gallego J. Microstructural characterization of layers produced by plasma nitriding on austenitic and superaustenitic stainless steel grades. J ASTM Int 2012;9:1–11.
[17] Raghavan V. The Cr–Fe–N–Ni system. J Phase Equilib 1997;18:158–72.
[18] He Y, Li Z, Qi H, Gao W. Standard free energy change of formation per unit volume: a new parameter for evaluating nucleation and growth of oxides, sulphides, carbides and nitrides. Mater Res Innov 1997;1:157–60.
[19] Mitchell DRG, Attard DJ, Collins GA, Short KT. Characterization of PI3 and RF plasma nitrided austenitic stainless steels using plan and cross-sectional TEM techniques. Surf Coat Technol 2003;165:107–18.
[20] Xu X, Wang L, Yu Z, Qiang J, Hei Z. Study of microstructure of low-temperature plasma-nitrided AISI 304 stainless steel. Metall Mater Trans A 2000;31A:1193–9.
[21] Collins GA, Hutchings R, Short KT, Tendys J, Li X, Samandi M. Nitriding of austenitic stainless steel by plasma immersion ion implantation. Surf Coat Technol 1995;74/75:417–24.
[22] Fernandes FAP, Casteletti LC, Totten GE, Gallego J. Decomposition of expanded austenite in AISI 316L stainless steel nitrided at 723 K. Int Heat Treat Surf Eng 2012;6:103–6.